Stellar ages, masses and radii from asteroseismic modelling are robust to systematic errors in spectroscopy

E. P. Bellinger[1],[*], S. Hekker[2,1], G. C. Angelou[3], A. Stokholm[1], and S. Basu[4]

[1] Stellar Astrophysics Centre, Department of Physics and Astronomy, Aarhus University, Denmark
e-mail: bellinger@phys.au.dk
[2] Stellar Ages & Galactic Evolution (SAGE) Group, Max Planck Institute for Solar System Research, Göttingen, Germany
[3] Max Planck Institute for Astrophysics, Garching, Germany
[4] Department of Astronomy, Yale University, New Haven, Connecticut, USA

ABSTRACT

Context. The search for twins of the Sun and Earth relies on accurate characterization of stellar and exoplanetary parameters: i.e., ages, masses, and radii. In the modern era of asteroseismology, parameters of solar-like stars are derived by fitting theoretical models to observational data, which include measurements of their oscillation frequencies, metallicity [Fe/H], and effective temperature $T_{\rm eff}$. Combining this information with transit data furthermore yields the corresponding parameters for their associated exoplanets.
Aims. While values of [Fe/H] and $T_{\rm eff}$ are commonly stated to a precision of ~ 0.1 dex and ~ 100 K, the impact of systematic errors in their measurement have not been studied in practice within the context of the parameters derived from them. Here we seek to quantify this.
Methods. We use the *Stellar Parameters in an Instant* (SPI) pipeline to estimate the parameters of nearly 100 stars observed by *Kepler* and *Gaia*, many of which are confirmed planet hosts. We adjust the reported spectroscopic measurements of these stars by introducing faux systematic errors and, separately, artificially increasing the reported uncertainties of the measurements, and quantify the differences in the resulting parameters.
Results. We find that a systematic error of 0.1 dex in [Fe/H] translates to differences of only 4%, 2%, and 1% on average in the resulting stellar ages, masses, and radii, which are well within their uncertainties ($\sim 11\%$, 3.5%, 1.4%) as derived by SPI. We also find that increasing the uncertainty of [Fe/H] measurements by 0.1 dex increases the uncertainties of the ages, masses, and radii by only 0.01 Gyr, 0.02 $\rm M_\odot$, and 0.01 $\rm R_\odot$, which are again well below their reported uncertainties (~ 0.5 Gyr, 0.04 $\rm M_\odot$, 0.02 $\rm R_\odot$). The results for $T_{\rm eff}$ at 100 K are similar.
Conclusions. Stellar parameters from SPI are unchanged within uncertainties by errors of up to 0.14 dex or 175 K, and are even more robust to errors in $T_{\rm eff}$ than the seismic scaling relations. Consequently, the parameters for their exoplanets are robust as well.

Key words. Asteroseismology — stars: abundances, low-mass, evolution, oscillations (including pulsations) — planets and satellites: fundamental parameters

1. Introduction

The modern study of cool dwarf stars has been revolutionized in recent years by ultraprecise measurements of low-amplitude global stellar pulsations (for a summary of early results, see Chaplin & Miglio 2013). Traveling through the star before emerging near the surface, pulsations bring information to light about the otherwise opaque conditions of the stellar interior, and thereby provide numerous constraints to the internal structure and composition of stars. Indeed, connecting theoretical stellar models to measurements of pulsation frequencies—as well as other measurements, such as those derived from spectroscopy—yields precise determinations of stellar parameters such as age, mass, and radius (for an overview, see Basu & Chaplin 2017).

Precisely constrained stellar parameters are broadly useful for a variety of endeavours, such as testing theories of stellar and galactic evolution (e.g., Deheuvels et al. 2016; Hjørringgaard et al. 2017; Nissen et al. 2017; Bellinger et al. 2017) and mapping out history and dynamics of the Galaxy (e.g., Chiappini et al. 2015; Anders et al. 2017; Silva Aguirre et al. 2018; Feuillet et al. 2018). Combining stellar parameters with transit measurements furthermore yields properties of the exoplanets that they harbor, such as their masses, radii, obliquities, eccentricities, and semi-major axes (e.g., Seager & Mallén-Ornelas 2003; Huber et al. 2013; Van Eylen et al. 2015; Huber 2016, 2018; Campante et al. 2016; Kamiaka et al. 2018; Adibekyan et al. 2018). This then permits tests to theories of planet formation (e.g., Lin et al. 1996; Watson et al. 2011; Morton & Johnson 2011; Lai et al. 2011; Guillochon et al. 2011; Thies et al. 2011; Teyssandier et al. 2013; Plavchan & Bilinski 2013; Matsakos & Königl 2015, 2017; Li & Winn 2016; Königl et al. 2017; Gratia & Fabrycky 2017) and facilitates the search for habitable exoplanets.

From first principles, one may obtain approximate relations to deduce stellar radii (R), mean densities (ρ), and masses (M) from asteroseismic data by scaling the values of the Sun to the observed properties of other stars ("scaling relations," Ulrich 1986; Brown et al. 1991; Kjeldsen & Bedding 1995):

$$\frac{R}{\rm R_\odot} \simeq \left(\frac{\nu_{\rm max}}{\nu_{\rm max,\odot}}\right)\left(\frac{\Delta\nu}{\Delta\nu_\odot}\right)^{-2}\left(\frac{T_{\rm eff}}{T_{\rm eff,\odot}}\right)^{\frac{1}{2}} \tag{1}$$

$$\frac{\rho}{\rho_{\odot}} \simeq \left(\frac{\Delta\nu}{\Delta\nu_{\odot}}\right)^2 \left(\frac{T_{\text{eff}}}{T_{\text{eff},\odot}}\right) \tag{2}$$

$$\frac{M}{\text{M}_{\odot}} \simeq \left(\frac{\nu_{\max}}{\nu_{\max,\odot}}\right)^3 \left(\frac{\Delta\nu}{\Delta\nu_{\odot}}\right)^{-4} \left(\frac{T_{\text{eff}}}{T_{\text{eff},\odot}}\right)^{\frac{3}{2}}. \tag{3}$$

Here T_{eff} is the effective temperature of the star, $\nu_{\max}$ is the frequency of maximum oscillation power, and $\Delta\nu$ is the large frequency separation (for detailed definitions, see, e.g., Basu & Chaplin 2017). The quantities subscripted with the solar symbol ($\odot$) correspond to the solar values: $\nu_{\max,\odot} = 3090 \pm 30 \, \mu\text{Hz}$, $\Delta\nu_{\odot} = 135.1 \pm 0.1 \, \mu\text{Hz}$, and $T_{\text{eff},\odot} = 5772.0 \pm 0.8$ K (Huber et al. 2011; Prša et al. 2016). This way of estimating stellar parameters is often referred to as the "direct method" (e.g., Lundkvist et al. 2018) because it is independent of stellar models and relies only on physical arguments. Note that there are no such scaling relations for the stellar age.

The seismic scaling relations are all functions of the stellar effective temperature, which, along with metallicity, can be derived from spectroscopic observations of a star. A variety of factors go into the determination of these spectroscopic parameters, such as spectra normalization, corrections for pixel-to-pixel variations, the placement of the continuum, and so on (e.g., Massey & Hanson 2013; Škoda 2017). The analysis can be complicated by effects such as line blending and broadening. Uncertainties in atmospheric models and the techniques for obtaining atmospheric parameters such as the measurement of equivalent widths, fitting on synthetic spectra, and degeneracies between spectroscopic parameters can also cause difficulties. Often, parameters for targets in large spectroscopic surveys are extracted automatically without visual inspection, which can lead to poor fits that sometimes go unnoticed. Conversely, analysis based on visual inspection sometimes leads to different practitioners coming to different conclusions about the same star. There are thus opportunities for systematic errors to be introduced into the determined effective temperatures and metallicities (e.g., Creevey et al. 2013). However, to date, no study has systematically tested in practice the impact of systematic errors in spectroscopic parameters on the determination of stellar parameters for a large sample of stars.

Unlike the effective temperature, the classical scaling relations presented above are not functions of metallicity, and so one would expect metallicity to have little role in the determination of stellar masses and radii. However, these relations are approximations, and are not perfectly accurate. Several studies (e.g., White et al. 2011; Belkacem et al. 2011; Mathur et al. 2012; Hekker et al. 2013; Mosser et al. 2013; Huber et al. 2014; Guggenberger et al. 2016; Sharma et al. 2016; Gaulme et al. 2016; Huber et al. 2017; Guggenberger et al. 2017; Viani et al. 2017; Themeßl et al. 2018) have sought to quantify the validity of the seismic scaling relations—especially as a function of stellar evolution, when the assumption of solar homology breaks down—for example by comparison with stellar models, or via orbital analyses of binary stars. Viani et al. (2017) have also recently shown theoretically that these relations neglect a term for the mean molecular weight, which implies a previously unaccounted for dependence on metallicity.

To obtain more accurate mass and radius estimates—and stellar ages—one can fit theoretical models to the observations of a star (e.g., Brown et al. 1994; Gai et al. 2011; Metcalfe et al. 2014; Lebreton & Goupil 2014; Silva Aguirre et al. 2015, 2017; Bellinger et al. 2016). The connection between observations and stellar parameters then becomes much more complex, relying on the details of not only the coupled differential equations governing the structure and evolution of stars, but also the choices and

implementations regarding the microphysics of the star, such as the opacities and equation of state of stellar plasma. This motivates the need for numerical studies to determine the relationships between the observations of a star and the resulting fundamental parameters (e.g., Brown et al. 1994; Angelou et al. 2017; Valle et al. 2018). Here we examine one important aspect of these relations: namely, the impact of systematic errors and underestimated uncertainties in spectroscopic parameters on the determination of stellar parameters via asteroseismic modelling.

In order to perform this study, we use the *Stellar Parameters in an Instant* pipeline (SPI, Bellinger et al. 2016), which uses machine learning to rapidly connect observations of stars to theoretical models. The SPI method involves training an ensemble or "forest" of decision tree regressors (Breiman 2001; Geurts et al. 2006; Friedman et al. 2001) to learn the relationships between the observable aspects of stars (such as their oscillations) and the unobserved or unobservable aspects (such as their age). We then feed the observations of a particular star into the learned forest, which outputs the desired predicted quantities. In order to propagate the uncertainties of the observations into each of the predicted quantities, we generate random realizations of noise according to the uncertainties of the observations (including their correlations), and run these random realizations through the forest as well. This yields the posterior distribution for each predicted quantity, from which we may obtain, for example, the mean value and its corresponding uncertainty for quantities such as the stellar age, mass, radius, mean density, and luminosity.

Using this approach, one can simultaneously and independently vary multiple free parameters corresponding to uncertain aspects of stellar models, such as the efficiency of convection and the strength of gravitational settling; and therefore propagate many of the uncertainties of the theoretical models into the resulting stellar parameters. To this end, we generated a large grid of stellar models that have been varied in age as well as seven other parameters controlling the physics of the evolution, which is described in more detail in the next section. Since obtaining the parameters of a star with SPI takes less than a minute (rather than hours or days, as is typical with some other methods) we are then able to test the robustness of the final stellar parameters against injections of various amounts of systematic errors.

1.1. Implications for exoplanets

The question of how systematic errors in spectroscopy impact stellar parameter determinations has direct bearing on exoplanet research. This is due to the fact that the determination of exoplanetary parameters generally depends very strongly on the ability to constrain the parameters of the host star (see Figure 1).

Given the radius of the host star from asteroseismology (e.g., using Equation 1; or using more sophisticated methods, such as SPI), and assuming a uniformly bright stellar disk, the radius of a transiting exoplanet can be found by measuring the transit depth (e.g., Seager & Mallén-Ornelas 2003). Given the stellar radius and mean density (e.g., Equation 2), and assuming a circular orbit, one can compute the semi-major axis of an exoplanet from its orbital period. Combining that information with the stellar mass (e.g., Equation 3), one can find the mass of an exoplanet using Kepler's third law. As prevailing theories give that planets form roughly around the same time as the host star, the stellar age that is found is generally then attributed to its companions as well (e.g., Jenkins et al. 2015; Campante et al. 2015; Safonova et al. 2016; Christensen-Dalsgaard & Silva Aguirre 2018). From this information, the composition of an exoplanet can be determined by connecting these properties to theoretical models of planet
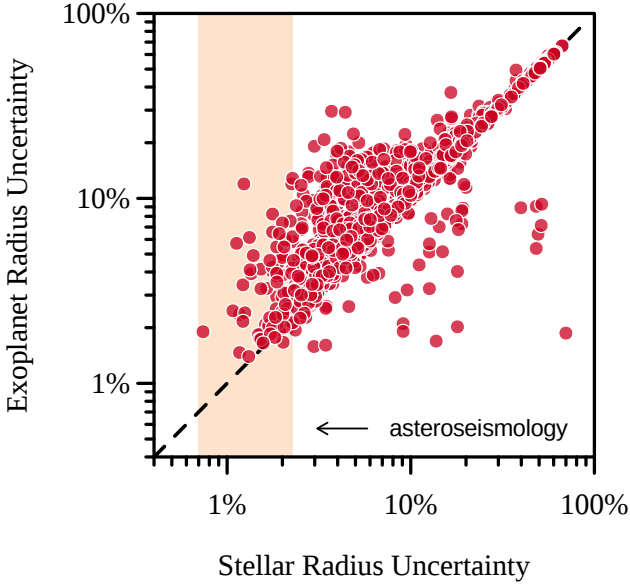
Fig. 1: Relative uncertainties of the radii of transiting exoplanets as a function of the relative uncertainty in the radius of their host star. The dashed line shows 1-to-1 agreement. The shaded region shows the full range of stellar radii uncertainties determined for the 97 stars examined in this paper. Exoplanet data are taken from the collection by Han et al. (2014).
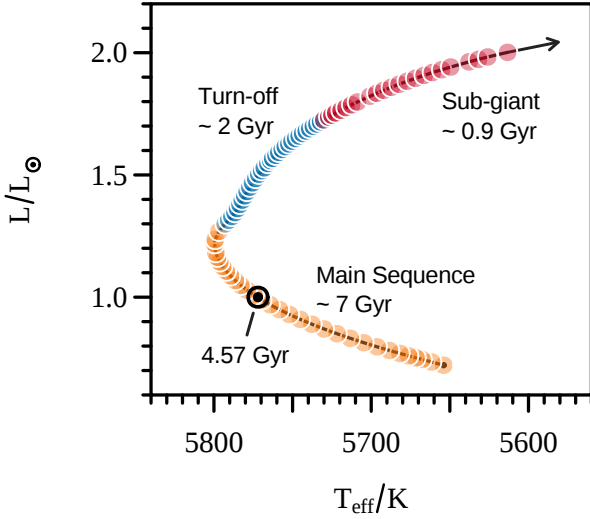
Fig. 2: Theoretical evolution of the Sun in the HR diagram. The position of the present-age Sun is given with the solar symbol (⊙). The points indicate models that have been selected from the track. They are colored according to their assigned phase of evolution, and the approximate duration of each phase is indicated.

structure and formation (e.g., Seager et al. 2007; Weiss & Marcy 2014; Rogers 2015; Huber 2018).

Thus, if the parameters derived for the host star are biased, then so too will be the parameters for its exoplanets. A differential bias—e.g., a bias that affects mass more than radius—would furthermore impact strongly on matters such as empirical mass–radius relations (e.g., Seager et al. 2007; Torres et al. 2010).

Table 1: Parameter ranges for the grid of stellar models. For reference, values corresponding to a solar-calibrated model and also the derived initial spectroscopic parameter ranges are listed as well.

Parameter	Symbol	Range	Solar Value
Mass	$M/M_\odot$	$(0.7, 1.8)$	1
Mixing Length	α_{MLT}	$(1, 3)$	1.85
Initial Helium	Y_0	$(0.22, 0.34)$	0.273
Initial Metallicity	Z_0	$(0.0001, 0.04)^a$	0.019
Overshoot	α_{ov}	$(0.0001, 1)^a$	-
Undershoot	α_{us}	$(0.0001, 1)^a$	$\leq 0.05^b$
Diffusion Factor	D	$(0.0001, 3)^a$	1
Eff. Temperature	T_{eff}	$(4000, 14000)$	5772
Metallicity	[Fe/H]	$(-2.2, 0.44)$	0

^{a}varied logarithmically, ^{b}Basu 1997

2. Methods

We used *Modules for Experiments in Stellar Astrophysics* (MESA r10108, Paxton et al. 2011, 2013, 2015, 2018) to construct a grid of stellar models following the procedure given by Bellinger et al. (2016). The initial parameters were varied quasi-randomly in the ranges given in Table 1. We introduced an additional free parameter, α_{uv}, which controls the efficiency of convective envelope undershooting. As convection is modelled in MESA as a time-dependent diffusive process, under- and overshooting are achieved by applying convective velocities to zones within a distance of αH_p beyond the convective boundary, where α is the under- or over-shooting parameter, and H_p is the local pressure scale height. The convective velocities that are used are taken from a distance f_0 before the boundary; here we used $f_0 = 0.01\, H_p$. The remaining aspects of the models are the same as in Bellinger et al. 2016.

We calculated $N = 8\,170$ evolutionary tracks which we simulated from the zero-age main sequence until either an age of 20 Gyr or an asymptotic period spacing of 150 s, which is generally around the base of the red giant branch. Since the initial conditions of the grid are varied quasi-randomly, the resolution in each parameter x is given by $(x_{\max} - x_{\min})/N$; e.g., the typical resolution in mass is approximately 0.0001 $M_\odot$. From each track we obtained 32 models with core hydrogen abundance $X_c > 0.1$ nearly evenly spaced in age (i.e., main-sequence models), 32 models with $0.1 \leq X_c \leq 10^{-6}$ nearly evenly spaced in $\log X_c$ (turn-off models), and 32 models beyond $X_c < 10^{-6}$ again nearly evenly spaced in age (sub-giant models). These phases are visualized in Figure 2.

We calculated p-mode frequencies for these models using the GYRE oscillation code (Townsend & Teitler 2013). We obtained frequency separations and ratios (Roxburgh & Vorontsov 2003) for these models following the procedures given in Bellinger et al. 2016. We removed models where the presence of mixed modes made it impossible to calculate these quantities.

3. Data

We obtained oscillation mode frequencies, $\nu_{\max}$ values, effective temperatures, and metallicities for 97 stars observed by the *Kepler* spacecraft (Borucki et al. 2010a) from previous studies. Data for 31 of the stars came from the *Kepler* Ages project (Silva Aguirre et al. 2015; Davies et al. 2016), and 66 were from the *Kepler* LEGACY project (Lund et al. 2017; Silva Aguirre et al. 2017). The spectroscopic parameters of these stars are visualized
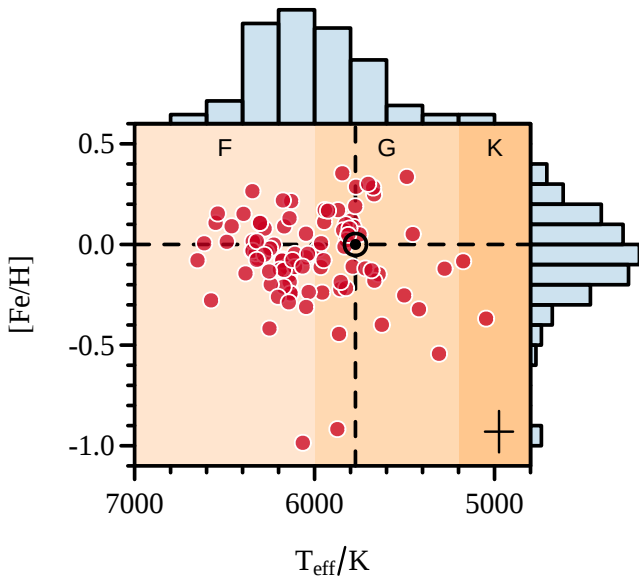
Fig. 3: Spectroscopic measurements of 97 solar-like oscillating stars observed by *Kepler*. Typical uncertainties (0.1 dex, 100 K) are indicated with the cross in the bottom right corner. Histograms are affixed to the top and right side of the figure showing the metallicity and effective temperature distributions for the sample. The values for the Sun are given with the solar symbol ($\odot$). The background colors indicate the spectral type (F, G, K).

in Figure 3. We processed the mode frequencies to obtain asteroseismic frequency separations and ratios in the same way that we processed the theoretical model frequencies in the previous section. These stars are visualized in the so-called 'CD Diagram' (Christensen-Dalsgaard 1984) in Figure 4. The relative uncertainties on the observational constraints for these stars are visualized in Figure 5. This figure furthermore illustrates the observational data that we input into SPI.

For comparison purposes, we additionally obtained luminosity and radius measurements for these stars from the recent *Gaia* Data Release 2 (DR2, Gaia Collaboration et al. 2018; Andrae et al. 2018). We identified these stars using the 2MASS cross-matched catalog (Marrese et al. 2018) for all except KIC 10514430 and KIC 8379927, which we located using a cone search. We note that these measurements have not been corrected for extinction.

4. Results

We applied SPI to the sample of 97 stars using the grid of theoretical models that we generated and the observational constraints shown in Figure 5. Random realizations of the observations that fell outside of the range of the grid of models were dropped. Figure 6 shows the relative uncertainties in the estimated stellar parameters for this sample. The stellar parameters themselves can be found in Table A.1 in the Appendix. Figure 7 shows the positions of these stars on the Hertzsprung–Russell diagram using effective temperatures from spectroscopy and predicted luminosities from SPI.

The accuracy of SPI can be gauged by comparing its predictions with observations. In Figure 8 we show a comparison of predicted luminosities and radii to those from *Gaia* DR2. Again we find good agreement, despite the systematic errors that may currently be present in the *Gaia* data. Sahlholdt & Silva Aguirre

(2018) recently compared their predicted radii to *Gaia* radii for these stars as well and found similar results, although our estimates are in somewhat better agreement, in the sense that we find fewer discrepant stars. Most likely this is due to the fact that our models incorporate a greater variety of mixing length parameters, which is important for determining stellar radii. We furthermore compare the results from SPI to the BASTA models for these stars (Silva Aguirre et al. 2015, 2017) in Figure 9, finding good agreement.

The stellar parameters we derive using SPI can be used to check the validity of the seismic scaling relations (Equations 1, 2, 3). Figure 10 shows a comparison between the masses, radii, and mean densities obtained in these two ways. Overall, there is good agreement, albeit with some significant outliers. It is worth noting that two of the discrepant stars—KIC 8760414 and KIC 7106245 (labels 8 and 10 in the Figure)—are two of the lowest mass stars and are by far the most metal poor stars of the sample, with [Fe/H] values of approximately -0.9 dex and -1 dex, respectively. In contrast, the next most metal poor star has a metallicity of approximately -0.5 dex (*cf.* Figure 3). However, we find no apparent metallicity dependence in the residuals of any of the scaling relations. We note that the large number of outliers in mean density estimates in Figure 10 arise mainly from their very small uncertainties. Only one of the labelled outliers, KIC 8478994 is a confirmed planet host (label 9 in the Figure—see Table A.1).

4.1. Testing systematic errors in spectroscopy

We performed two sets of tests aimed at gauging the robustness of stellar parameters to unreliable spectroscopic parameters. In the first test, we biased all of the spectroscopic measurements by systematically changing their reported metallicities and effective temperatures (both independently and simultaneously). We then measured the extent to which their estimated radii, masses, mean densities, and ages changed with respect to the unperturbed estimates of the stellar parameter. In the second test, we increased the reported random uncertainties for each star and measured the change to the uncertainties of the resulting stellar parameters.

The results of these experiments are shown in Figures 11, 12, 13, 14, 15, and 16. There it can be seen that a systematic error of 0.1 dex in [Fe/H] measurements translates on average to differences of only 4%, 2%, and 1% in the resulting stellar ages, masses, and radii, respectively. These differences are smaller than the reported relative uncertainties for these quantities ($\sim$ 11%, 3.5%, 1.4%). Similarly, a systematic error of 100 K in effective temperature results in relative differences of 6%, 2%, and 0.4%. Furthermore, increasing the reported uncertainty of [Fe/H] measurements by 0.1 dex (100%) increases the uncertainties of stellar ages, masses, and radii on average by only 0.01 Gyr, 0.02 $M_\odot$, and 0.01 $R_\odot$, which are well below the reported uncertainties for these estimates ($\sim$ 0.5 Gyr, 0.04 $M_\odot$, 0.02 $R_\odot$). Similarly, increasing the reported uncertainty of $T_{\rm eff}$ by 100 K increases the uncertainties of the estimated stellar parameters by 0.2 Gyr, 0.01 $M_\odot$, and 0.003 $R_\odot$. Thus, even relatively large systematic errors and increases to uncertainty result in essentially the same stellar parameters.

When biasing [Fe/H] estimates by more than 0.1 dex (1σ), some of the stellar metallicities went beyond the grid of models and were dropped. By 0.5 dex (5σ), only half of the stars remained, and that is where we stopped the experiment. We found that in order for the relative differences in the resulting stellar ages, masses, and radii to be equal to their reported uncertainties, [Fe/H] ($T_{\rm eff}$) measurements would need to be biased by at
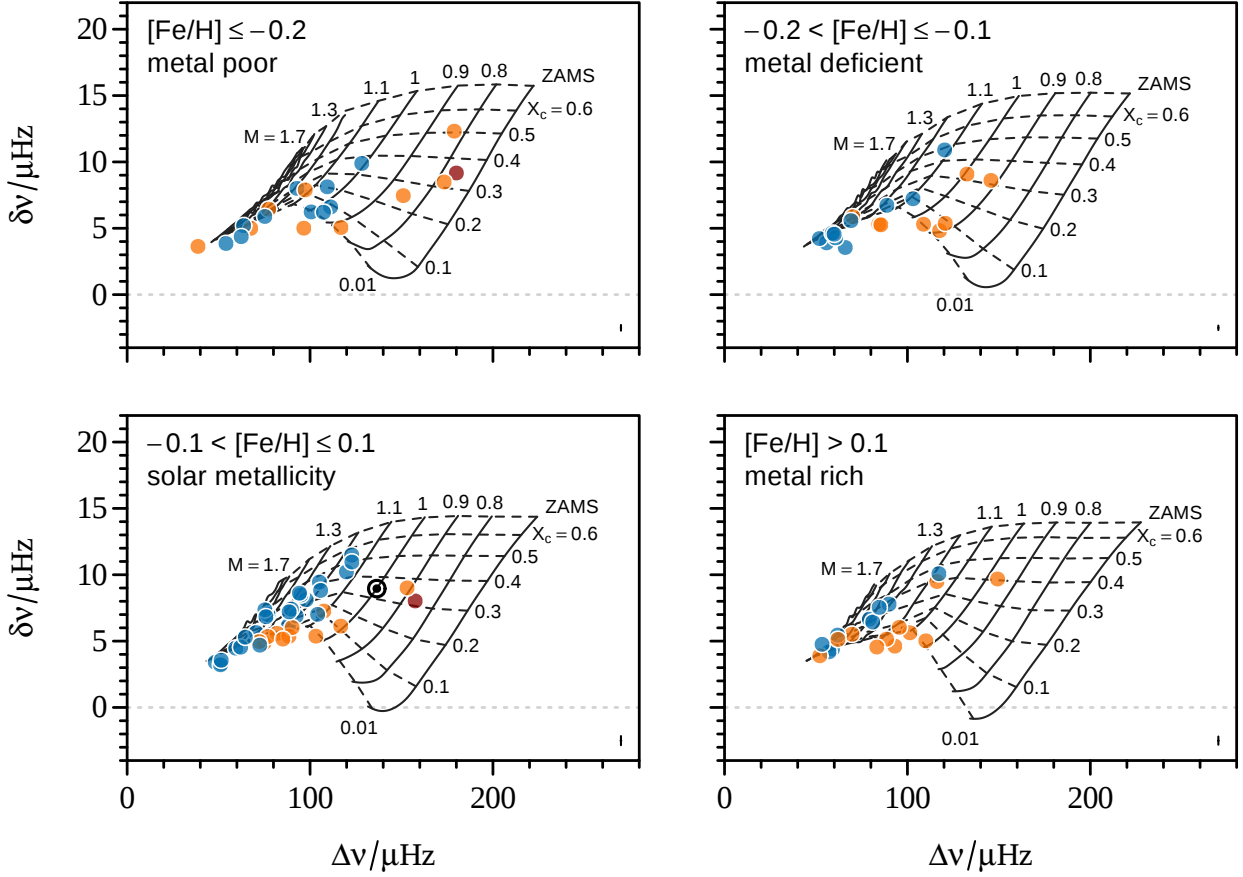
Fig. 4: CD diagram showing asteroseismic measurements—the small frequency separation $\delta\nu$ and the the large frequency separation $\Delta\nu$—for the sample of 97 solar-like stars studied here. The panels are arranged by metallicity. The points are colored by spectral type: F (blue, $T_{eff} > 6000$ K), G (orange, $6000 \geq T_{eff} > 5200$ K), K (red, $T_{eff} \leq 5200$ K). The cross in the bottom right corner of each panel shows typical uncertainties (see also Figure 5). The dotted light gray line indicates where $\delta\nu = 0$. The solid lines trace theoretical tracks of stellar evolution, with each track labelled along the top by its mass (in solar units) and connected by the dashed lines that are spaced in core-hydrogen abundance (X_c).

least 0.24 dex (175 K), 0.14 dex (200 K), and 0.14 dex (300 K), respectively.

The results regarding the uncertainties are consistent with the theoretical findings of Angelou et al. (2017, their Fig. 7). Though our analysis was done using frequency ratios to account for the surface term, Basu & Kinnane (2018) have similarly shown that how the surface term is accounted for does not affect estimates of the global properties (but see also Aarslev et al. 2017).

The tests regarding effective temperatures also show these biases propagated through the seismic scaling relations (Equations 1, 2, 3). We find that estimates obtained using SPI are even more robust to systematic errors than the scaling relations.

5. Conclusions

We estimated the stellar parameters of 97 main-sequence and early sub-giant stars observed by the *Kepler* spacecraft using the SPI pipeline. We compared the estimates of stellar mass, radius, and mean density that we obtained from stellar modelling for these stars to the estimates from seismic scaling relations and found good agreement. We found no evidence in the residuals for

a trend with metallicity. We similarly compared the estimates of stellar radius and luminosity that we obtained from stellar modelling to the measurements from *Gaia* DR2, and again found good agreement.

We used these stars to test the impact of systematic errors in metallicity and effective temperature on the determination of stellar age, mass, and radius via asteroseismic stellar modelling. We found that the resulting stellar parameters from SPI are stable with respect to even relatively large systematic errors in the spectroscopic measurements. We emphasize that these results are only valid for asteroseismic modelling performed using SPI; results from other methods may vary. We note that we have not tested the impact on more evolved stars, such as red giants, and there too the results may differ. We note also that there may be other sources of systematic errors in the theoretical models, such as the assumed opacities, nuclear reaction rates, and mixture of metals, which we have not examined here.

These results should not be taken to imply that spectroscopic measurements are unimportant. As was shown by Bellinger et al. (2016) and Angelou et al. (2017), metallicity measurements are consistently rated as being highly important for constraining stel-
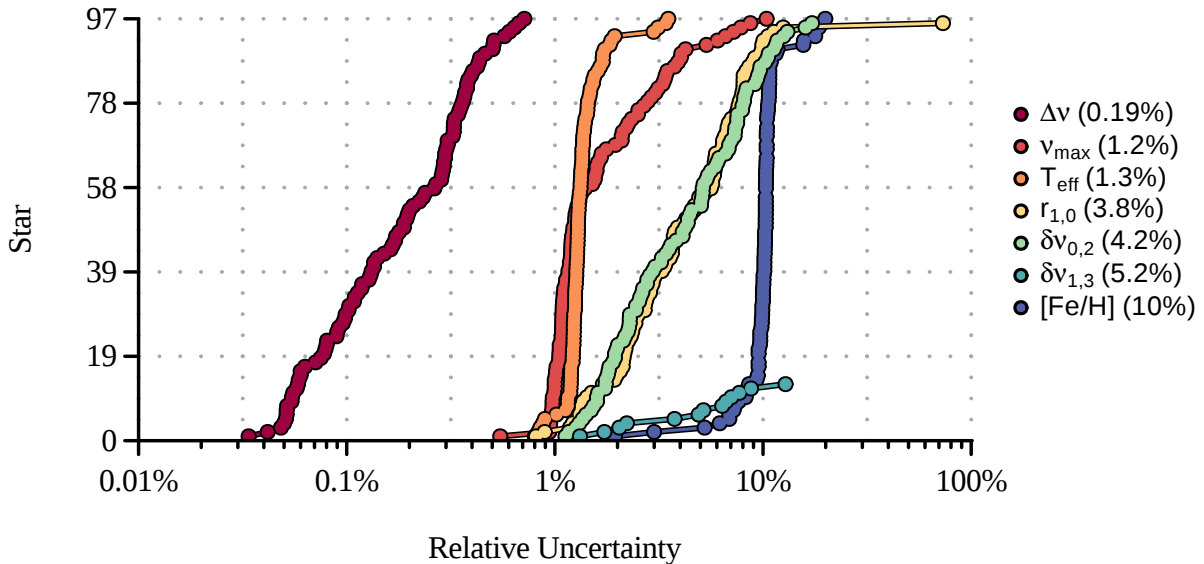
Fig. 5: Relative uncertainty of each measurement for each of the 97 stars analyzed here. The uncertainties are given in the sense of σ/μ where μ is the mean of the estimate and σ is the standard deviation—except in the case of [Fe/H], where these quantities are instead given for exp([Fe/H]). For each type of measurement, the order of the stars is given in order of increasing relative uncertainty, so for example 'Star 1' is not necessarily the same star between all of the different types of measurements. Note that $\delta\nu_{1,3}$ measurements are only available for 13 of the stars.
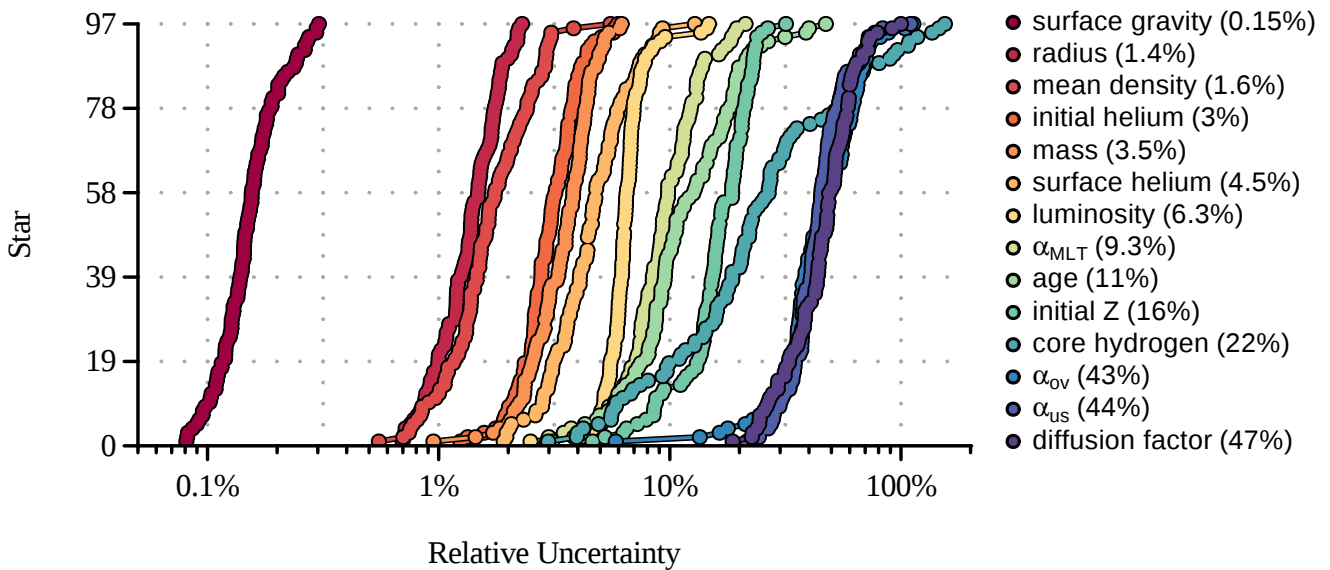
Fig. 6: Cumulative distributions showing the relative uncertainty of each estimated stellar parameter for each of the 97 stars, obtained by running the data in Figure 5 through SPI.

lar models, as they provide unique information that is not redundant with the oscillation data. However, measurements of stellar metallicity are most important in constraining aspects of the models related to the initial chemical composition and mixing processes that take place during the evolution. They are however of comparatively less importance in constraining global parameters such as the stellar age, mass, and radius from existing stellar models, as these quantities are well-constrained by seismology.

We conclude that asteroseismic modelling is a very reliable technique for obtaining ages, masses, radii, and other parameters of solar-like oscillators on the main sequence. Consequently, the parameters for their exoplanets, being that they are based on these values, are robust to such systematics as well.

Fig. 7: Hertzsprung–Russell diagrams of solar-like stars with temperatures from spectroscopy and predicted luminosities from asteroseismic modelling. The panels are arranged by metallicity, with the lines showing theoretical evolutionary sequences for stars of the corresponding metallicities having the indicated masses (expressed in solar units). The dashed line traces the zero-age main sequence. The background colors indicate the spectral types of the stars (F, G, K). Typical uncertainties are 0.15 $L_\odot$ and 100 K.
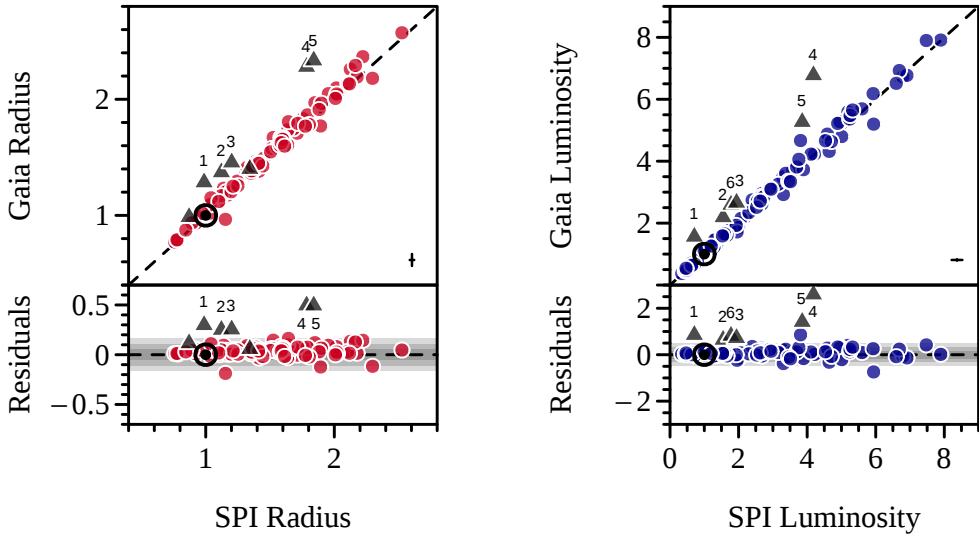
Fig. 8: Comparison of stellar radii (left) and luminosities (right) in solar units from *Gaia* observations against those from stellar modelling using the SPI pipeline. Typical uncertainties are shown as error bars in the lower right corners. Each shade of gray in the residual plots represents an *average* 1σ, ranging from 1 to 3. Stars with estimates significantly different at the $\sigma > 3$ level are shown as gray triangles. Stars which are outliers in more than one panel are labelled. Note the differences in scale between the left and right panels. The biases in the residuals are consistent with zero (-0.056 ± 0.091 $R_\odot$ and -0.14 ± 0.36 $L_\odot$)
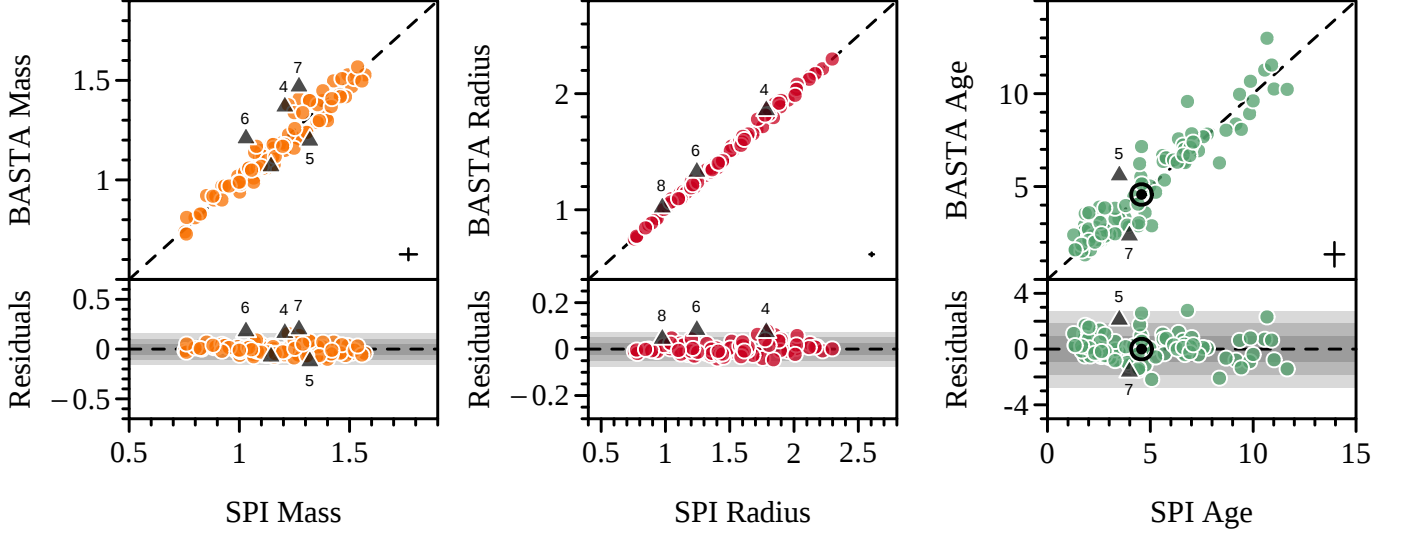
Fig. 9: Comparison of stellar masses (in solar units), radii (in solar units), and ages (in Gyr) determined via stellar modelling using BASTA against those from stellar modelling using SPI. The biases in the residuals are all consistent with zero (0.001 ± 0.061 M$_\odot$, -0.001 ± 0.027 R$_\odot$, and -0.1 ± 1.0 Gyr).
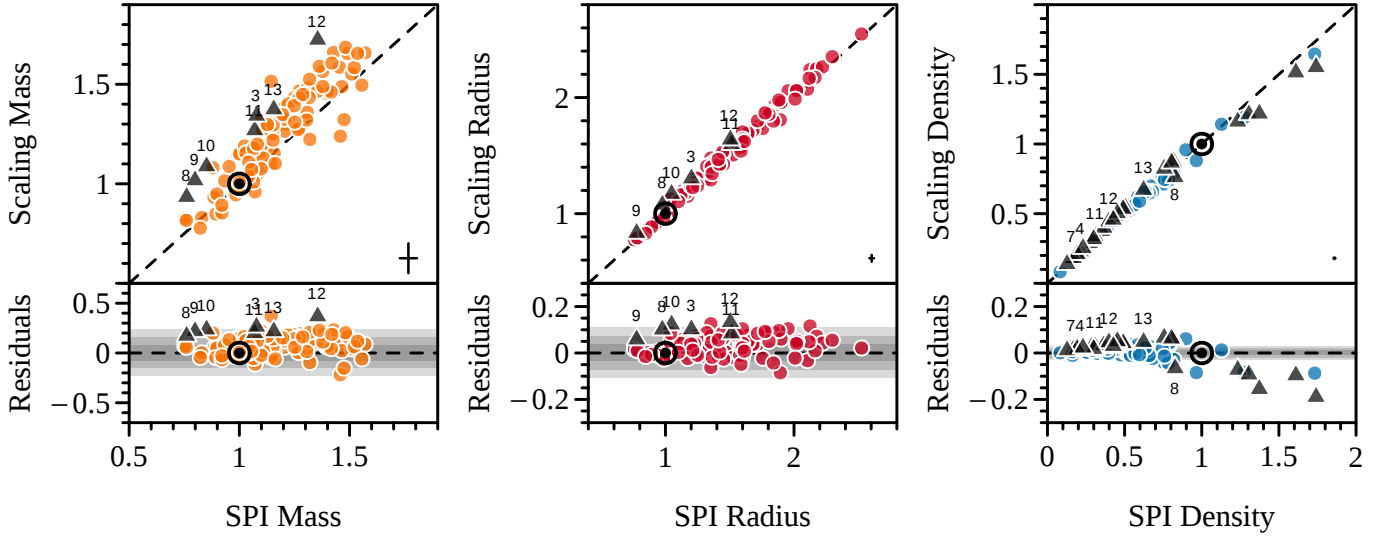

Fig. 10: Comparison of stellar masses, radii, and mean densities (in solar units) determined via the seismic scaling relations (Equations 1, 2, 3) against those from stellar modelling using the SPI pipeline. The biases in the residuals are all consistent with zero (0.09 ± 0.11 M$_\odot$, 0.035 ± 0.045 R$_\odot$, and 0.005 ± 0.042 $\rho_\odot$).
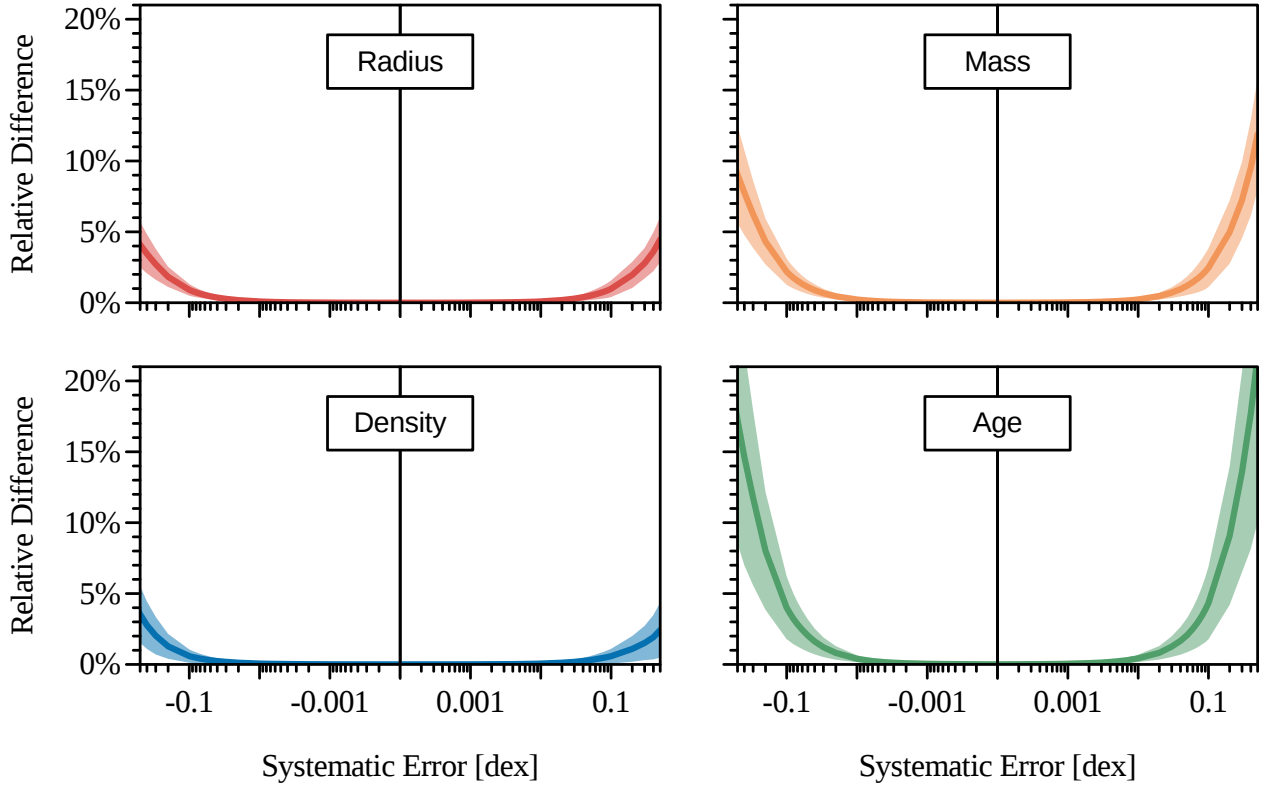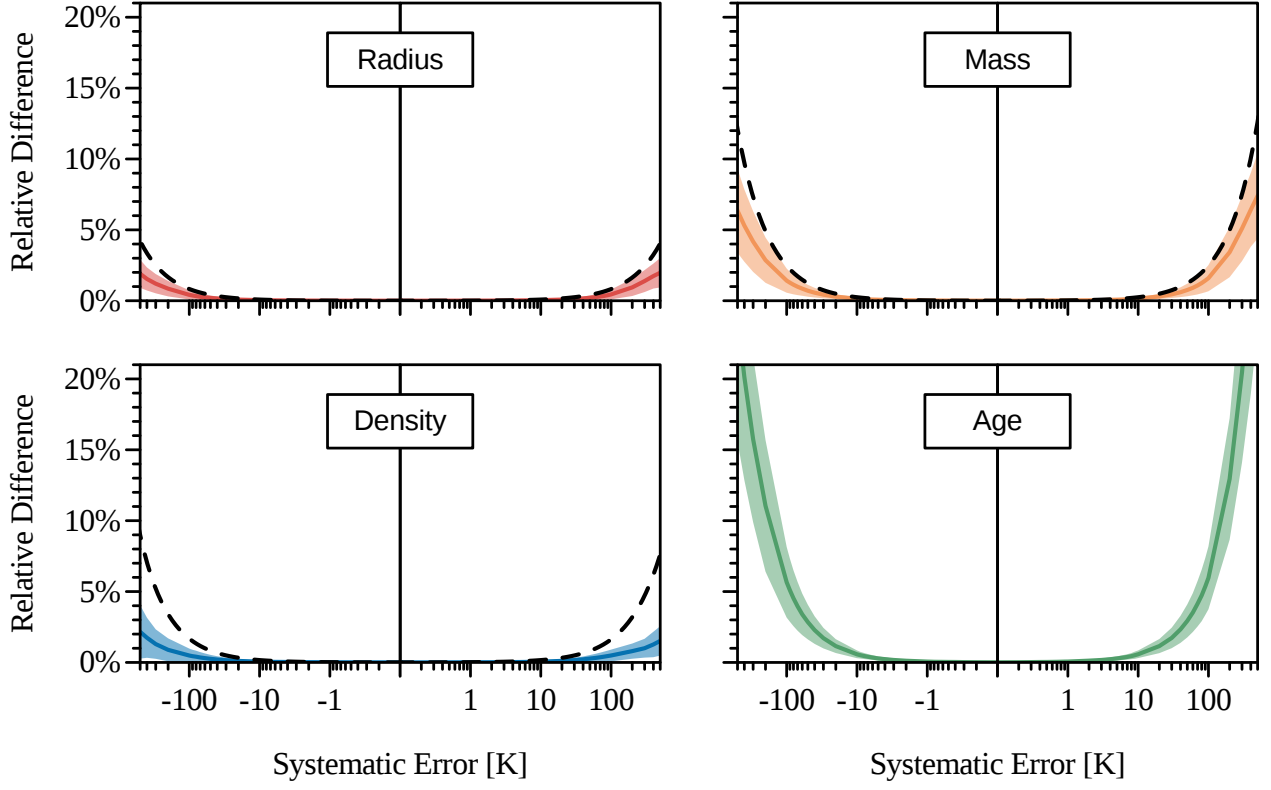
Fig. 11: Average relative differences in stellar parameter estimates (radius, mass, density, and stellar age) between estimates made using the reported measurements and estimates made using [Fe/H] values that have been biased with systematic errors ranging from -0.5 dex to 0.5 dex. The lines show the mean value and the shaded regions show the standard deviation across the 97 stars.
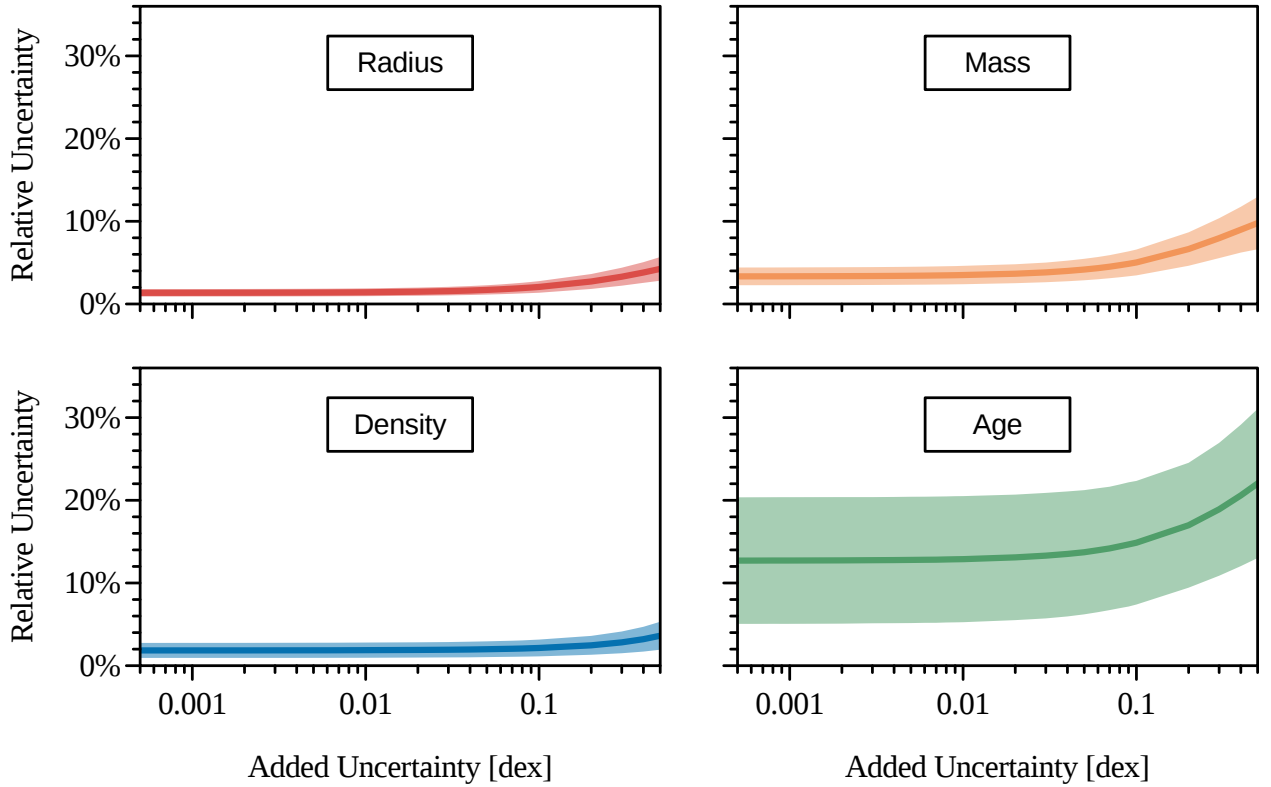
Fig. 12: Average relative uncertainties in stellar parameter estimates (radius, mass, mean density, and stellar age) as a function of the amount of additional random uncertainty given to [Fe/H] measurements ranging logarithmically from 0.0005 dex to 0.5 dex.
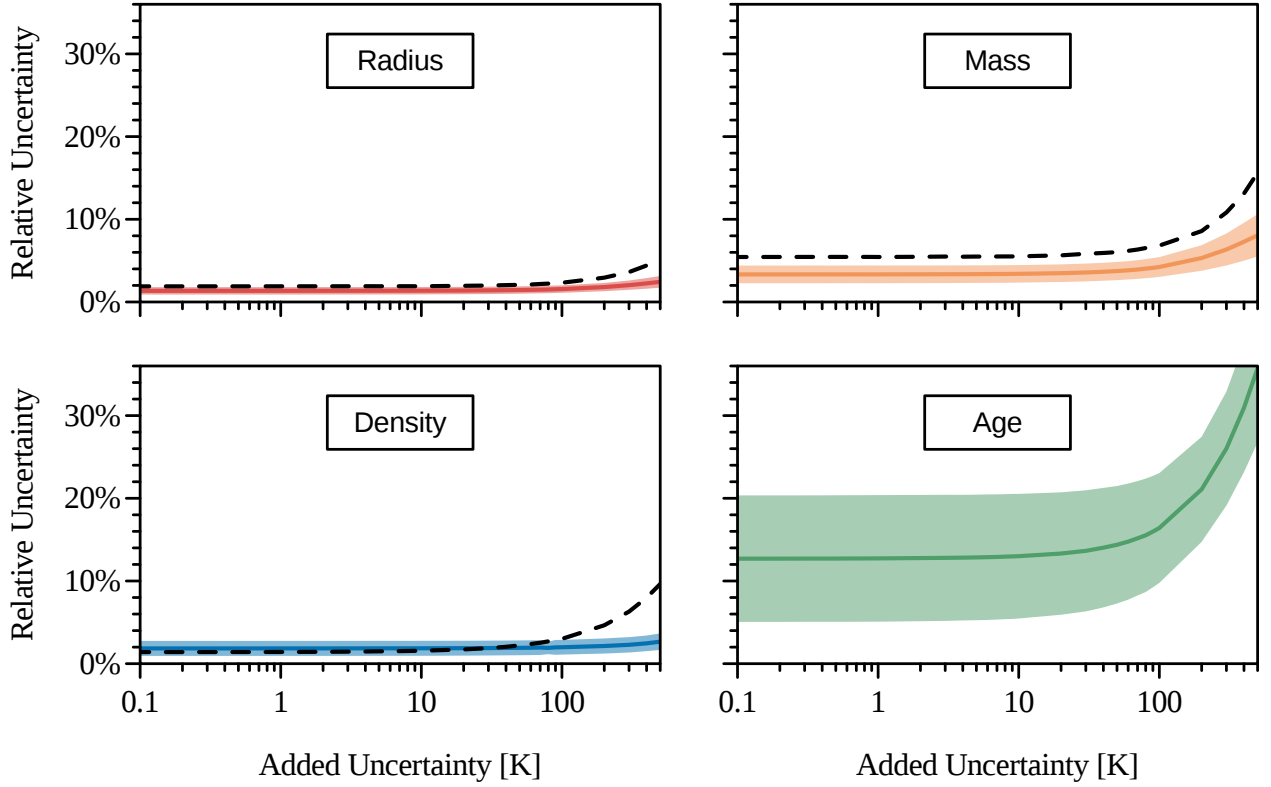
Fig. 13: Average relative differences in stellar parameter estimates (radius, mass, mean density, and stellar age) between estimates made using the reported measurements and estimates made using T_{eff} values that have been biased with systematic errors ranging from -500 K to 500 K. The dashed lines show the relative differences from the seismic scaling relations (Equations 1, 2 and 3).
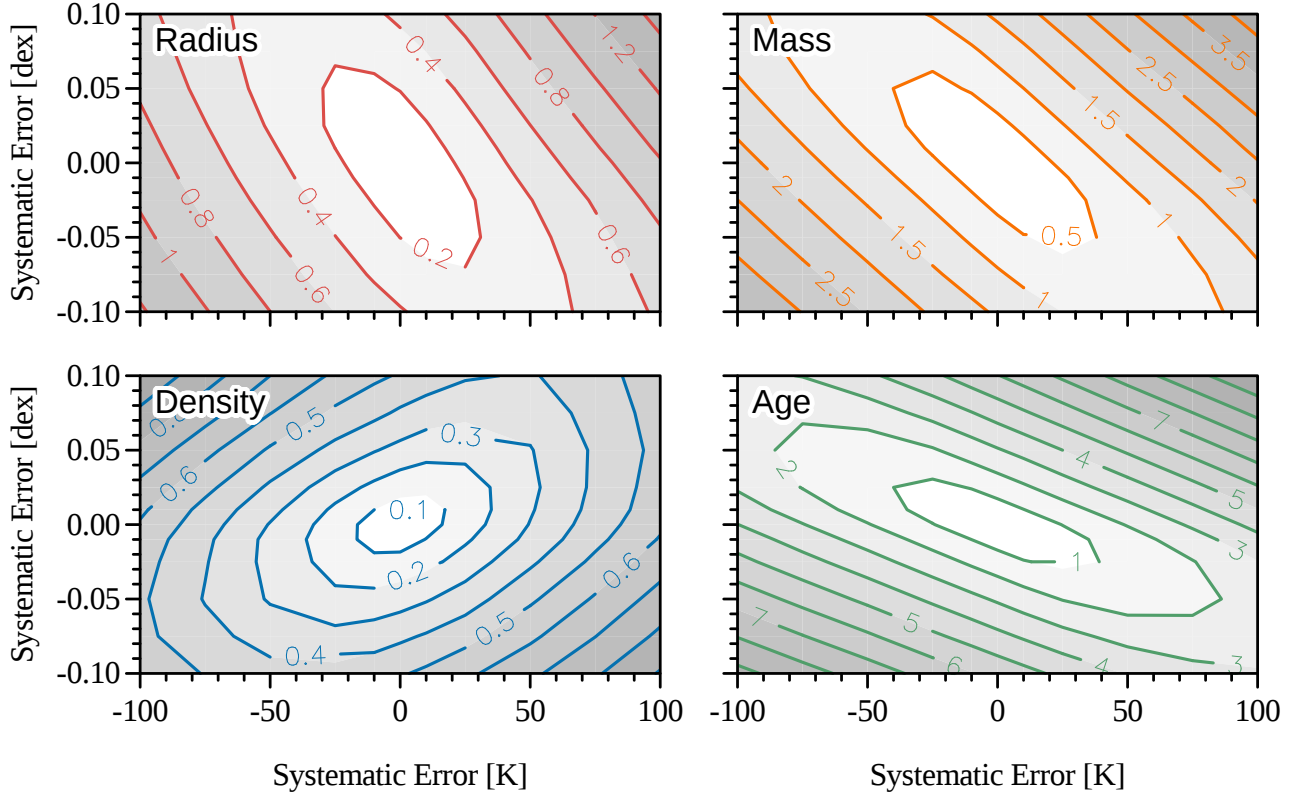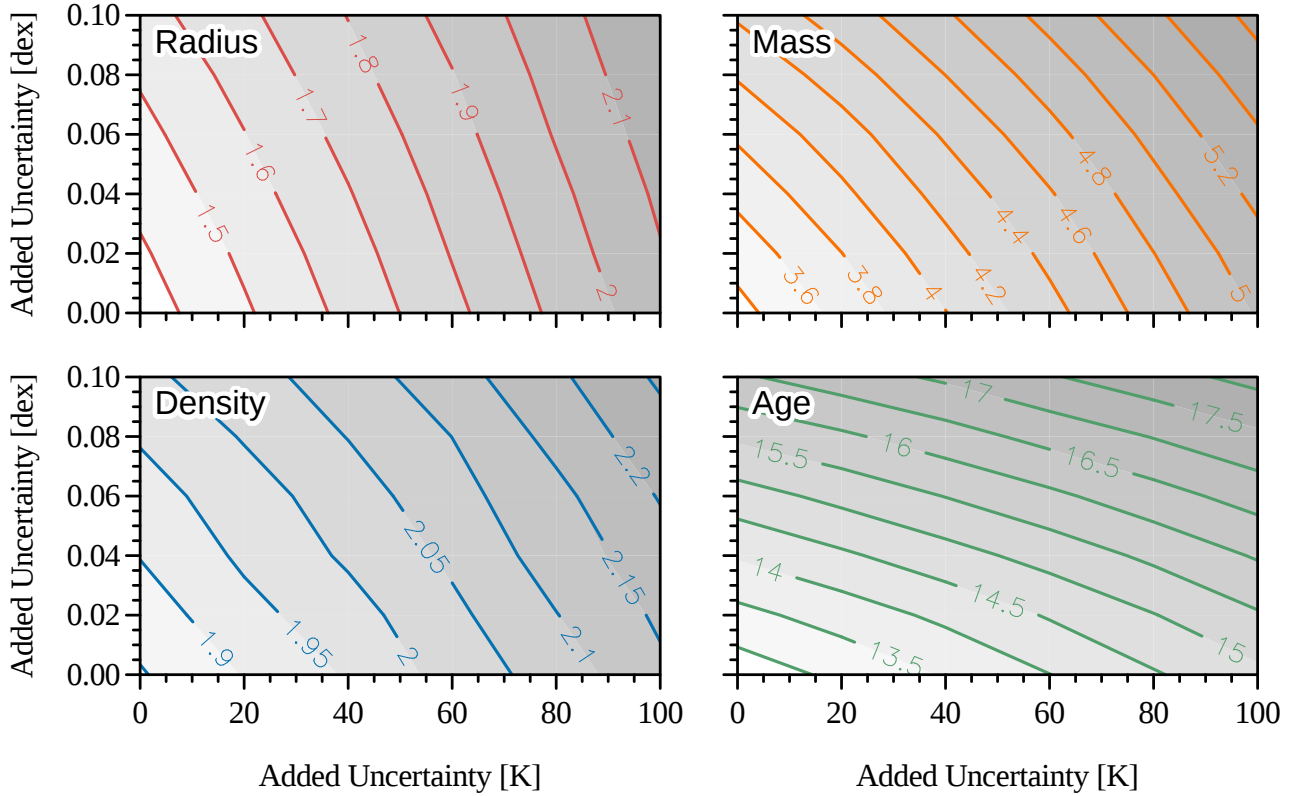

Fig. 14: Average relative uncertainties in stellar parameter estimates (radius, mass, mean density, and stellar age) as a function of the amount of additional random uncertainty given to T_{eff} measurements ranging logarithmically from 0.1 K to 500 K.

Fig. 15: Average relative differences (in percent) in stellar parameter estimates (radius, mass, mean density, and stellar age) between estimates made using the reported measurements and estimates made using (simultaneously) systematically biased [Fe/H] and $T_{\rm eff}$ values.

Fig. 16: Average relative uncertainties (in percent) in stellar parameter estimates (radius, mass, mean density, and stellar age) as a function of the amount of additional random uncertainty given to [Fe/H] and $T_{\rm eff}$ measurements.

Appendix A: Stellar Parameters

Table A.1: Stellar parameters for the *Kepler* Ages and LEGACY stars from the SPI pipeline: age, mass, radius, mean density, luminosity, and number of confirmed exoplanets. The labels next to some of the KIC numbers refer to the outliers highlighted in Figure 10 and 8. The footnotes in the planets column refer to the publication that announced or confirmed their discovery.

KIC	τ/Gyr	$M/\mathrm{M}_\odot$	$R/\mathrm{R}_\odot$	$\rho/\rho_\odot$	$L/\mathrm{L}_\odot$	Planets
1435467	2.03 ± 0.37	1.396 ± 0.033	1.712 ± 0.018	0.2789 ± 0.0045	4.22 ± 0.21	
2837475	1.34 ± 0.51	1.455 ± 0.061	1.638 ± 0.022	0.331 ± 0.010	4.62 ± 0.30	
3425851	3.77 ± 0.58	1.145 ± 0.049	1.354 ± 0.020	0.4625 ± 0.0062	2.67 ± 0.17	
3427720	2.34 ± 0.23	1.108 ± 0.032	1.121 ± 0.010	0.7904 ± 0.0079	1.527 ± 0.079	
3456181	2.62 ± 0.37	1.428 ± 0.062	2.125 ± 0.035	0.1489 ± 0.0027	6.79 ± 0.38	
3544595	6.63 ± 0.64	0.885 ± 0.038	0.924 ± 0.016	1.128 ± 0.025	0.804 ± 0.058	2[a]
3632418	3.40 ± 0.37	1.271 ± 0.047	1.849 ± 0.026	0.2008 ± 0.0020	4.59 ± 0.33	1[b]
3656476	9.16 ± 0.80	1.079 ± 0.027	1.318 ± 0.017	0.4749 ± 0.0095	1.62 ± 0.11	
3735871	1.81 ± 0.26	1.108 ± 0.032	1.109 ± 0.010	0.816 ± 0.014	1.535 ± 0.063	
4141376	3.48 ± 0.56	0.993 ± 0.041	1.038 ± 0.013	0.897 ± 0.031	1.365 ± 0.094	1[c]
4143755	10.56 ± 0.52	0.898 ± 0.019	1.414 ± 0.013	0.3211 ± 0.0036	1.85 ± 0.11	
4349452	2.47 ± 0.55	1.206 ± 0.055	1.312 ± 0.023	0.535 ± 0.011	2.40 ± 0.15	3[a,d]
4914423	5.60 ± 0.68	1.117 ± 0.059	1.468 ± 0.021	0.3546 ± 0.0058	2.29 ± 0.14	2[a]
4914923	6.37 ± 0.33	1.123 ± 0.033	1.388 ± 0.014	0.4207 ± 0.0042	2.00 ± 0.11	
5094751	5.63 ± 0.79	1.072 ± 0.041	1.353 ± 0.019	0.4346 ± 0.0098	2.09 ± 0.13	2[a]
5184732	4.84 ± 0.35	1.205 ± 0.022	1.3427 ± 0.0085	0.5034 ± 0.0050	1.912 ± 0.098	
5773345	2.24 ± 0.50	1.510 ± 0.044	2.017 ± 0.021	0.1841 ± 0.0026	5.19 ± 0.33	
5866724	2.53 ± 0.42	1.273 ± 0.032	1.423 ± 0.017	0.4434 ± 0.0064	2.648 ± 0.098	3[e]
5950854	9.8 ± 1.1	0.984 ± 0.044	1.236 ± 0.023	0.524 ± 0.012	1.62 ± 0.14	
6106415	4.98 ± 0.50	1.069 ± 0.038	1.219 ± 0.018	0.596 ± 0.011	1.78 ± 0.12	
6116048	6.80 ± 0.63	1.002 ± 0.031	1.218 ± 0.014	0.5602 ± 0.0080	1.78 ± 0.11	
6196457	4.5 ± 1.0	1.268 ± 0.069	1.756 ± 0.029	0.2359 ± 0.0042	3.29 ± 0.25	3[f,g]
6225718[13]	3.02 ± 0.51	1.156 ± 0.043	1.234 ± 0.016	0.6230 ± 0.0082	2.19 ± 0.13	
6278762	10.90 ± 0.86	0.753 ± 0.012	0.7588 ± 0.0045	1.741 ± 0.023	0.343 ± 0.022	5[h]
6508366	2.49 ± 0.19	1.492 ± 0.052	2.177 ± 0.032	0.1446 ± 0.0024	6.91 ± 0.47	
6521045	6.44 ± 0.35	1.091 ± 0.031	1.525 ± 0.011	0.3090 ± 0.0034	2.43 ± 0.14	3[a]
6603624	7.77 ± 0.45	1.065 ± 0.023	1.173 ± 0.012	0.668 ± 0.016	1.283 ± 0.059	
6679371	2.13 ± 0.12	1.570 ± 0.030	2.222 ± 0.017	0.1432 ± 0.0018	7.90 ± 0.44	
6933899	6.61 ± 0.28	1.104 ± 0.023	1.599 ± 0.012	0.2712 ± 0.0020	2.67 ± 0.18	
7103006	2.09 ± 0.45	1.482 ± 0.056	1.954 ± 0.026	0.1985 ± 0.0038	5.60 ± 0.38	
7106245[10]	8.36 ± 0.72	0.851 ± 0.025	1.048 ± 0.014	0.752 ± 0.017	1.363 ± 0.098	
7199397	3.63 ± 0.33	1.308 ± 0.034	2.526 ± 0.028	0.0821 ± 0.0014	6.69 ± 0.29	
7206837	1.80 ± 0.55	1.400 ± 0.041	1.584 ± 0.016	0.3516 ± 0.0052	3.58 ± 0.18	
7296438	6.60 ± 0.40	1.158 ± 0.034	1.405 ± 0.017	0.4187 ± 0.0045	2.00 ± 0.11	
7510397[4]	3.97 ± 0.35	1.206 ± 0.030	1.784 ± 0.015	0.2127 ± 0.0017	4.18 ± 0.28	
7670943	2.36 ± 0.47	1.309 ± 0.046	1.447 ± 0.019	0.4336 ± 0.0055	3.31 ± 0.27	
7680114	7.57 ± 0.85	1.108 ± 0.033	1.411 ± 0.022	0.398 ± 0.011	2.07 ± 0.14	
7771282	3.28 ± 0.56	1.353 ± 0.064	1.681 ± 0.032	0.2866 ± 0.0049	3.89 ± 0.23	
7871531	9.34 ± 0.58	0.830 ± 0.022	0.870 ± 0.011	1.274 ± 0.025	0.632 ± 0.040	
7940546	2.80 ± 0.20	1.317 ± 0.026	1.899 ± 0.018	0.1924 ± 0.0025	4.96 ± 0.24	
7970740	10.67 ± 0.36	0.760 ± 0.014	0.7819 ± 0.0055	1.610 ± 0.013	0.444 ± 0.029	
8006161	4.75 ± 0.25	1.004 ± 0.020	0.9353 ± 0.0070	1.233 ± 0.011	0.717 ± 0.040	
8077137	4.48 ± 0.62	1.150 ± 0.043	1.638 ± 0.027	0.2626 ± 0.0056	3.37 ± 0.25	2[f]
8150065	3.28 ± 0.55	1.196 ± 0.066	1.393 ± 0.032	0.445 ± 0.011	2.57 ± 0.20	
8179536	1.84 ± 0.37	1.248 ± 0.059	1.353 ± 0.027	0.5039 ± 0.0081	2.68 ± 0.20	
8228742	4.42 ± 0.49	1.221 ± 0.069	1.791 ± 0.041	0.2128 ± 0.0030	4.11 ± 0.36	
8292840	2.79 ± 0.54	1.099 ± 0.036	1.321 ± 0.015	0.4789 ± 0.0060	2.40 ± 0.16	3[i]

[a] Marcy et al. 2014
[b] Howell et al. 2012
[c] Haywood et al. 2018
[d] Steffen et al. 2012
[e] Chaplin et al. 2013
[f] Xie 2014
[g] Van Eylen & Albrecht 2015
[h] Campante et al. 2015
[i] Rowe et al. 2014

Table A.1 (continued from previous page)

KIC	τ/Gyr	M/M$_\odot$	R/R$_\odot$	ρ/$\rho_\odot$	L/L$_\odot$	Planets
8349582	8.68 ± 0.53	1.144 ± 0.015	1.4520 ± 0.0066	0.3742 ± 0.0072	2.003 ± 0.086	1[a]
8379927[2]	1.84 ± 0.29	1.105 ± 0.049	1.122 ± 0.017	0.790 ± 0.012	1.55 ± 0.13	
8394589	4.20 ± 0.39	1.024 ± 0.037	1.153 ± 0.023	0.673 ± 0.019	1.70 ± 0.11	
8424992	10.00 ± 0.94	0.893 ± 0.038	1.033 ± 0.025	0.819 ± 0.027	1.034 ± 0.083	
8478994[9]	5.68 ± 0.96	0.799 ± 0.017	0.776 ± 0.014	1.732 ± 0.063	0.482 ± 0.032	4[j,k]
8494142	2.09 ± 0.32	1.458 ± 0.056	1.893 ± 0.025	0.2149 ± 0.0060	4.64 ± 0.33	2[f]
8554498[5]	3.49 ± 0.41	1.320 ± 0.026	1.840 ± 0.017	0.2126 ± 0.0030	3.86 ± 0.17	
8684730	2.55 ± 0.45	1.475 ± 0.039	2.105 ± 0.039	0.163 ± 0.011	5.01 ± 0.25	
8694723[11]	5.26 ± 0.23	1.070 ± 0.023	1.515 ± 0.013	0.3084 ± 0.0039	3.16 ± 0.19	
8760414[8]	15.78 ± 0.91	0.761 ± 0.011	0.9755 ± 0.0090	0.828 ± 0.015	1.032 ± 0.064	
8866102	1.81 ± 0.27	1.223 ± 0.054	1.357 ± 0.022	0.4902 ± 0.0048	2.66 ± 0.16	
8938364	11.02 ± 0.58	0.995 ± 0.023	1.363 ± 0.011	0.3955 ± 0.0046	1.74 ± 0.10	
9025370[1]	5.77 ± 0.60	0.921 ± 0.035	0.987 ± 0.019	0.965 ± 0.019	0.709 ± 0.084	
9098294	9.42 ± 0.85	0.934 ± 0.041	1.112 ± 0.027	0.682 ± 0.021	1.301 ± 0.081	
9139151	1.82 ± 0.19	1.205 ± 0.044	1.168 ± 0.016	0.7566 ± 0.0097	1.96 ± 0.12	
9139163	2.09 ± 0.28	1.378 ± 0.039	1.557 ± 0.017	0.3653 ± 0.0038	3.70 ± 0.22	
9206432[12]	1.67 ± 0.42	1.355 ± 0.047	1.505 ± 0.021	0.3982 ± 0.0065	3.76 ± 0.21	
9353712	2.44 ± 0.21	1.465 ± 0.054	2.164 ± 0.032	0.1446 ± 0.0019	6.60 ± 0.50	
9410862	7.34 ± 0.75	0.954 ± 0.028	1.139 ± 0.017	0.650 ± 0.019	1.580 ± 0.099	
9414417	2.80 ± 0.22	1.319 ± 0.041	1.882 ± 0.023	0.1978 ± 0.0026	4.89 ± 0.29	
9592705	2.21 ± 0.19	1.521 ± 0.044	2.118 ± 0.026	0.1610 ± 0.0036	5.94 ± 0.37	
9812850	1.99 ± 0.39	1.417 ± 0.057	1.805 ± 0.025	0.2399 ± 0.0067	4.71 ± 0.24	
9955598	6.69 ± 0.48	0.921 ± 0.032	0.893 ± 0.012	1.306 ± 0.015	0.634 ± 0.042	1[a]
9965715[6]	3.88 ± 0.49	1.030 ± 0.023	1.244 ± 0.011	0.538 ± 0.013	1.78 ± 0.17	
10068307[7]	3.98 ± 0.34	1.271 ± 0.045	2.024 ± 0.023	0.1546 ± 0.0015	5.24 ± 0.37	
10079226	2.56 ± 0.40	1.153 ± 0.050	1.160 ± 0.016	0.744 ± 0.013	1.521 ± 0.088	
10162436	3.29 ± 0.42	1.379 ± 0.052	2.019 ± 0.026	0.1678 ± 0.0017	5.25 ± 0.31	
10454113[3]	5.07 ± 0.91	1.078 ± 0.048	1.202 ± 0.022	0.659 ± 0.018	1.94 ± 0.13	
10514430	7.01 ± 0.61	1.042 ± 0.029	1.578 ± 0.016	0.2664 ± 0.0034	2.55 ± 0.16	
10516096	6.66 ± 0.47	1.108 ± 0.035	1.422 ± 0.017	0.3861 ± 0.0029	2.30 ± 0.17	
10586004	6.13 ± 0.89	1.154 ± 0.041	1.643 ± 0.029	0.2605 ± 0.0056	2.73 ± 0.20	2[i]
10644253	1.28 ± 0.25	1.128 ± 0.027	1.1204 ± 0.0085	0.804 ± 0.012	1.525 ± 0.060	
10666592	2.02 ± 0.25	1.556 ± 0.046	2.009 ± 0.023	0.1918 ± 0.0027	5.92 ± 0.42	1[l]
10730618	4.4 ± 1.1	1.249 ± 0.085	1.716 ± 0.053	0.251 ± 0.012	3.81 ± 0.52	
10963065	4.57 ± 0.48	1.065 ± 0.043	1.225 ± 0.026	0.584 ± 0.017	1.93 ± 0.13	1[a]
11081729	1.66 ± 0.84	1.363 ± 0.039	1.444 ± 0.018	0.4526 ± 0.0082	3.46 ± 0.20	
11133306	4.58 ± 0.74	1.081 ± 0.040	1.198 ± 0.016	0.634 ± 0.015	1.66 ± 0.11	
11253226	1.34 ± 0.50	1.420 ± 0.071	1.599 ± 0.026	0.3468 ± 0.0094	4.53 ± 0.29	
11295426	6.31 ± 0.39	1.099 ± 0.031	1.251 ± 0.013	0.5673 ± 0.0080	1.587 ± 0.096	3[m]
11401755	6.94 ± 0.78	1.043 ± 0.031	1.601 ± 0.026	0.2552 ± 0.0074	2.91 ± 0.21	2[n]
11772920	9.9 ± 1.1	0.823 ± 0.040	0.845 ± 0.018	1.373 ± 0.024	0.468 ± 0.068	
11807274	2.01 ± 0.28	1.306 ± 0.032	1.597 ± 0.013	0.3223 ± 0.0052	3.51 ± 0.17	2[o]
11853905	6.60 ± 0.57	1.163 ± 0.046	1.588 ± 0.019	0.2911 ± 0.0042	2.53 ± 0.17	1[p]
11904151	11.65 ± 0.93	0.880 ± 0.031	1.041 ± 0.016	0.784 ± 0.022	0.995 ± 0.054	2[q,r]
12009504	3.80 ± 0.29	1.197 ± 0.044	1.411 ± 0.018	0.4266 ± 0.0054	2.63 ± 0.16	
12069127	2.31 ± 0.18	1.537 ± 0.051	2.297 ± 0.030	0.1267 ± 0.0015	7.48 ± 0.44	
12069424	6.92 ± 0.25	1.056 ± 0.019	1.213 ± 0.011	0.5967 ± 0.0085	1.531 ± 0.076	
12069449	7.08 ± 0.22	1.0000 ± 0.0086	1.101 ± 0.012	0.758 ± 0.018	1.201 ± 0.024	1[s]
12258514	4.40 ± 0.29	1.252 ± 0.054	1.614 ± 0.023	0.2999 ± 0.0024	2.95 ± 0.18	
12317678	2.63 ± 0.28	1.288 ± 0.036	1.775 ± 0.022	0.2301 ± 0.0042	5.33 ± 0.25	

[j] Hadden & Lithwick 2014
[k] Barclay et al. 2013
[l] Pál et al. 2008
[m] Gilliland et al. 2013
[n] Carter et al. 2012
[o] Steffen et al. 2013
[p] Borucki et al. 2010b
[q] Fressin et al. 2011
[r] Batalha et al. 2011
[s] Cochran et al. 1997

References

Aarslev, M. J., Christensen-Dalsgaard, J., Lund, M. N., Silva Aguirre, V., & Gough, D. 2017, in European Physical Journal Web of Conferences, Vol. 160, European Physical Journal Web of Conferences, 03010
Adibekyan, V., Sousa, S. G., & Santos, N. C. 2018, Asteroseismology and Exoplanets: Listening to the Stars and Searching for New Worlds, 49, 225
Akeson, R. L., Chen, X., Ciardi, D., et al. 2013, PASP, 125, 989
Anders, F., Chiappini, C., Rodrigues, T. S., et al. 2017, A&A, 597, A30
Andrae, R., Fouesneau, M., Creevey, O., et al. 2018, A&A, 616, A8
Angelou, G. C., Bellinger, E. P., Hekker, S., & Basu, S. 2017, ApJ, 839, 116
Barclay, T., Rowe, J. F., Lissauer, J. J., et al. 2013, Nature, 494, 452
Basu, S. 1997, MNRAS, 288, 572
Basu, S. & Chaplin, W. 2017, Asteroseismic Data Analysis: Foundations and Techniques, Princeton Series in Modern Obs (Princeton University Press)
Basu, S. & Kinnane, A. 2018, ArXiv e-prints [arXiv:1810.07205]
Batalha, N. M., Borucki, W. J., Bryson, S. T., et al. 2011, ApJ, 729, 27
Belkacem, K., Goupil, M. J., Dupret, M. A., et al. 2011, A&A, 530, A142
Bellinger, E. P., Angelou, G. C., Hekker, S., et al. 2016, ApJ, 830, 31
Bellinger, E. P., Basu, S., Hekker, S., & Ball, W. H. 2017, ApJ, 851, 80
Borucki, W. J., Koch, D., Basri, G., et al. 2010a, Science, 327, 977
Borucki, W. J., Koch, D. G., Brown, T. M., et al. 2010b, ApJ, 713, L126
Breiman, L. 2001, Machine Learning, 45, 5
Brown, T. M., Christensen-Dalsgaard, J., Weibel-Mihalas, B., & Gilliland, R. L. 1994, ApJ, 427, 1013
Brown, T. M., Gilliland, R. L., Noyes, R. W., & Ramsey, L. W. 1991, ApJ, 368, 599
Campante, T. L., Barclay, T., Swift, J. J., et al. 2015, ApJ, 799, 170
Campante, T. L., Lund, M. N., Kuszlewicz, J. S., et al. 2016, ApJ, 819, 85
Carter, J. A., Agol, E., Chaplin, W. J., et al. 2012, Science, 337, 556
Chaplin, W. J. & Miglio, A. 2013, ARA&A, 51, 353
Chaplin, W. J., Sanchis-Ojeda, R., Campante, T. L., et al. 2013, ApJ, 766, 101
Chiappini, C., Anders, F., Rodrigues, T. S., et al. 2015, A&A, 576, L12
Christensen-Dalsgaard, J. 1984, in Space Research in Stellar Activity and Variability, ed. A. Mangeney & F. Praderie, 11
Christensen-Dalsgaard, J. & Silva Aguirre, V. 2018, in Handbook of Exoplanets, ed. Deeg, Hans J. and Belmonte, Juan Antonio (Springer), 18
Cochran, W. D., Hatzes, A. P., Butler, R. P., & Marcy, G. W. 1997, ApJ, 483, 457
Creevey, O. L., Thévenin, F., Basu, S., et al. 2013, MNRAS, 431, 2419
Davies, G. R., Silva Aguirre, V., Bedding, T. R., et al. 2016, MNRAS, 456, 2183
Deheuvels, S., Brandão, I., Silva Aguirre, V., et al. 2016, A&A, 589, A93
Feuillet, D. K., Bovy, J., Holtzman, J., et al. 2018, MNRAS, 477, 2326
Fressin, F., Torres, G., Désert, J.-M., et al. 2011, ApJS, 197, 5
Friedman, J., Hastie, T., & Tibshirani, R. 2001, The Elements of Statistical Learning, Vol. 1 (Springer New York)
Gai, N., Basu, S., Chaplin, W. J., & Elsworth, Y. 2011, ApJ, 730, 63
Gaia Collaboration, Brown, A. G. A., Vallenari, A., et al. 2018, A&A, 616, A1
Gaulme, P., McKeever, J., Jackiewicz, J., et al. 2016, ApJ, 832, 121
Geurts, P., Ernst, D., & Wehenkel, L. 2006, Machine Learning, 63, 3
Gilliland, R. L., Marcy, G. W., Rowe, J. F., et al. 2013, ApJ, 766, 40
Ginsburg, A., Sipocz, B., Parikh, M., et al. 2018, astropy/astroquery: v0.3.7 release
Gratia, P. & Fabrycky, D. 2017, MNRAS, 464, 1709
Guggenberger, E., Hekker, S., Angelou, G. C., Basu, S., & Bellinger, E. P. 2017, MNRAS, 470, 2069
Guggenberger, E., Hekker, S., Basu, S., & Bellinger, E. 2016, MNRAS, 460, 4277
Guillochon, J., Ramirez-Ruiz, E., & Lin, D. 2011, ApJ, 732, 74
Hadden, S. & Lithwick, Y. 2014, ApJ, 787, 80
Han, E., Wang, S. X., Wright, J. T., et al. 2014, PASP, 126, 827
Haywood, R. D., Vanderburg, A., Mortier, A., et al. 2018, AJ, 155, 203
Hekker, S., Elsworth, Y., Mosser, B., et al. 2013, A&A, 556, A59
Hjørringgaard, J. G., Silva Aguirre, V., White, T. R., et al. 2017, MNRAS, 464, 3713
Howell, S. B., Rowe, J. F., Bryson, S. T., et al. 2012, ApJ, 746, 123
Huber, D. 2016, IAU Focus Meeting, 29, 620
Huber, D. 2018, Asteroseismology and Exoplanets: Listening to the Stars and Searching for New Worlds, 49, 119
Huber, D., Bedding, T. R., Stello, D., et al. 2011, ApJ, 743, 143
Huber, D., Carter, J. A., Barbieri, M., et al. 2013, Science, 342, 331
Huber, D., Silva Aguirre, V., Matthews, J. M., et al. 2014, ApJS, 211, 2
Huber, D., Zinn, J., Bojsen-Hansen, M., et al. 2017, ApJ, 844, 102
Jenkins, J. M., Twicken, J. D., Batalha, N. M., et al. 2015, AJ, 150, 56
Kamiaka, S., Benomar, O., & Suto, Y. 2018, MNRAS, 479, 391
Kjeldsen, H. & Bedding, T. R. 1995, A&A, 293, 87
Königl, A., Giacalone, S., & Matsakos, T. 2017, ApJ, 846, L13
Lai, D., Foucart, F., & Lin, D. N. C. 2011, MNRAS, 412, 2790
Lebreton, Y. & Goupil, M. J. 2014, A&A, 569, A21
Li, G. & Winn, J. N. 2016, ApJ, 818, 5
Lin, D. N. C., Bodenheimer, P., & Richardson, D. C. 1996, Nature, 380, 606
Lund, M. N., Silva Aguirre, V., Davies, G. R., et al. 2017, ApJ, 835, 172
Lundkvist, M. S., Huber, D., Silva Aguirre, V., & Chaplin, W. J. 2018, in Handbook of Exoplanets, ed. Deeg, Hans J. and Belmonte, Juan Antonio (Springer), 24
Marcy, G. W., Isaacson, H., Howard, A. W., et al. 2014, ApJS, 210, 20
Marrese, P. M., Marinoni, S., Fabrizio, M., & Altavilla, G. 2018, ArXiv e-prints [arXiv:1808.09151]
Massey, P. & Hanson, M. M. 2013, Astronomical Spectroscopy (Springer), 35
Mathur, S., Metcalfe, T. S., Woitaszek, M., et al. 2012, ApJ, 749, 152
Matsakos, T. & Königl, A. 2015, ApJ, 809, L20
Matsakos, T. & Königl, A. 2017, AJ, 153, 60
Metcalfe, T. S., Creevey, O. L., Doğan, G., et al. 2014, ApJS, 214, 27
Morton, T. D. & Johnson, J. A. 2011, ApJ, 729, 138
Mosser, B., Michel, E., Belkacem, K., et al. 2013, A&A, 550, A126
Nissen, P. E., Silva Aguirre, V., Christensen-Dalsgaard, J., et al. 2017, A&A, 608, A112
Pál, A., Bakos, G. Á., Torres, G., et al. 2008, ApJ, 680, 1450
Paxton, B., Bildsten, L., Dotter, A., et al. 2011, ApJS, 192, 3
Paxton, B., Cantiello, M., Arras, P., et al. 2013, ApJS, 208, 4
Paxton, B., Marchant, P., Schwab, J., et al. 2015, ApJS, 220, 15
Paxton, B., Schwab, J., Bauer, E. B., et al. 2018, ApJS, 234, 34
Plavchan, P. & Bilinski, C. 2013, ApJ, 769, 86
Prša, A., Harmanec, P., Torres, G., et al. 2016, AJ, 152, 41
Rogers, L. A. 2015, ApJ, 801, 41
Rowe, J. F., Bryson, S. T., Marcy, G. W., et al. 2014, ApJ, 784, 45
Roxburgh, I. W. & Vorontsov, S. V. 2003, A&A, 411, 215
Safonova, M., Murthy, J., & Shchekinov, Y. A. 2016, International Journal of Astrobiology, 15, 93
Sahlholdt, C. L. & Silva Aguirre, V. 2018, MNRAS, 481, L125
Seager, S., Kuchner, M., Hier-Majumder, C. A., & Militzer, B. 2007, ApJ, 669, 1279
Seager, S. & Mallén-Ornelas, G. 2003, ApJ, 585, 1038
Sharma, S., Stello, D., Bland-Hawthorn, J., Huber, D., & Bedding, T. R. 2016, ApJ, 822, 15
Silva Aguirre, V., Bojsen-Hansen, M., Slumstrup, D., et al. 2018, MNRAS, 475, 5487
Silva Aguirre, V., Davies, G. R., Basu, S., et al. 2015, MNRAS, 452, 2127
Silva Aguirre, V., Lund, M. N., Antia, H. M., et al. 2017, ApJ, 835, 173
Steffen, J. H., Fabrycky, D. C., Agol, E., et al. 2013, MNRAS, 428, 1077
Steffen, J. H., Fabrycky, D. C., Ford, E. B., et al. 2012, MNRAS, 421, 2342
Teyssandier, J., Terquem, C., & Papaloizou, J. C. B. 2013, MNRAS, 428, 658
Themeßl, N., Hekker, S., Southworth, J., et al. 2018, MNRAS, 478, 4669
Thies, I., Kroupa, P., Goodwin, S. P., Stamatellos, D., & Whitworth, A. P. 2011, MNRAS, 417, 1817
Torres, G., Andersen, J., & Giménez, A. 2010, A&A Rev., 18, 67
Townsend, R. H. D. & Teitler, S. A. 2013, MNRAS, 435, 3406
Ulrich, R. K. 1986, ApJ, 306, L37
Škoda, P. 2017, in Proceedings of EURO-VO Workshop Astronomical Spectroscopy and Virtual Observatory
Valle, G., Dell'Omodarme, M., Prada Moroni, P. G., & Degl'Innocenti, S. 2018, ArXiv e-prints [arXiv:1810.06997]
Van Eylen, V. & Albrecht, S. 2015, ApJ, 808, 126
Van Eylen, V., Lund, M. N., Silva Aguirre, V., et al. 2015, in European Physical Journal Web of Conferences, Vol. 101, European Physical Journal Web of Conferences, 02005
Viani, L. S., Basu, S., Chaplin, W. J., Davies, G. R., & Elsworth, Y. 2017, ApJ, 843, 11
Watson, C. A., Littlefair, S. P., Diamond, C., et al. 2011, MNRAS, 413, L71
Weiss, L. M. & Marcy, G. W. 2014, ApJ, 783, L6
White, T. R., Bedding, T. R., Stello, D., et al. 2011, ApJ, 743, 161
Xie, J.-W. 2014, ApJS, 210, 25